Hindawi
Mathematical Problems in Engineering
Volume 2021, Article ID 6153291, 12 pages
https://doi.org/10.1155/2021/6153291

Research Article

Stability Analysis of Multispan Pipeline Embedded in Temperature-Dependent Matrix

Nan Wu, Yongshou Liu, Guojun Tong, and Jiayin Dai

School of Mechanics, Civil Engineering and Architecture, Northwestern Polytechnical University, Xi'an 710129, China

Correspondence should be addressed to Guojun Tong; 381339861@qq.com

Received 2 June 2020; Revised 16 October 2020; Accepted 19 January 2021; Published 29 January 2021

Academic Editor: Aimé Lay-Ekuakille

In this paper, dynamic stiffness method is used to study the stability of multispan pipelines in temperature-dependent matrix. The effects of temperature changes and different span combinations on the natural frequency, critical velocity, and critical pressure of pipelines are discussed. The main conclusions are obtained and shown as follows. The increase of temperature will lead to the decrease of the first three order natural frequencies. The first two order critical velocities and critical pressure of the system will also decrease with increasing temperature. The change of span combination has no influence on the first-order critical velocity and first-order critical pressure of the system, but it has influence on the second order. The influence of the change of span combination on the first-order natural frequency is regular, but that on the second-order and third-order is not. The increase of the velocity will change the instability form of systems with different span combinations, while the change of the pressure inside the tube will not change the instability form of the system.

1. Introduction

As an important transportation and storage carrier of gas and liquid, pipeline plays an irreplaceable role in many fields such as aerospace, energy, and biological sciences. The research on pipeline stability is always a hot topic. Païdoussis and Li put forward that pipes' conveying fluid is a model dynamical problem [1]. Ibrahim and Li have made overviews about mechanics of pipes' conveying fluids [2, 3]. Zhang et al. studied the two parameters affecting the dynamics characteristics of a uniform conical-assembled pipe conveying fluid [4]. Ni et al. researched the natural frequency and stability analysis of a pipe conveying fluid with axially moving supports immersed in fluid [5]. Li et al. studied transient response of multispan pipe conveying fluid [6]. Yang et al. researched the adaptive vibration suppression of a pipe conveying fluid [7]. Xu and Jiao studied the axial vibration of a tube by interpolation [8].

In the application process, many pipelines are embedded in various matrices, and many scholars have studied relevant problems. Chang et al. researched flow-induced oscillations of a cantilevered pipe-conveying fluid with base excitation [9]. Lumentut and Friswell studied a smart pipe energy harvester excited by fluid flow and base excitation [10]. Elaikh et al. researched the dynamic behavior of cracked functionally graded material (FGM) pipe-conveying fluid [11]. Wang and Liu discussed the transverse vibration of FGM pipe-conveying fluid [12].

The temperature change of the system is a key factor in the stability analysis of the pipeline. Cao et al. studied the effect of two cases of temperature distributions on vibration of fluid-conveying functionally graded thin-walled pipes [13]. Raminnea et al. investigated nonlinear higher order Reddy theory for temperature-dependent vibration and instability of embedded functionally graded pipe-conveying fluid, nanoparticle mixture [14].

Compared with the existing literature, this paper innovatively introduces the concept of temperature-dependent matrix and considers the influence of coupling effect of variation in matrix elastic coefficient and axial force caused by temperature change on pipeline stability. We analyze the influence of not only temperature change but also different span combinations on the stability based on critical velocity

and pressure. The author hopes that this paper will help the application of pipeline engineering.

The structure of this paper can be summarized as follows: firstly, the governing equation of the pipeline is established based on Euler-Bernoulli beam theory, and then, the dynamic stiffness method is employed to solve the equation. Finally, the effects of temperature change and different span combinations on the natural frequency, critical velocity, and critical pressure of pipelines are discussed.

2. Vibration Governing Equation

The model of a multispan pipe embedded in the temperature-dependent matrix is demonstrated in Figure 1. The length of the multispan pipeline is $L_1 + L_2$. U stands for flow velocity. R_i and R_o stand for inner radius and outer radius, respectively. Based on Euler-Bernoulli beam model theory, the governing equation of the multispan pipe embedded in the temperature-varying matrix can be deduced as [15, 16]

$$\frac{\partial Q}{\partial x} = m\frac{\partial^2 w}{\partial t^2} + Kw - \frac{\partial}{\partial x}\left(N_x\frac{\partial w}{\partial x}\right) + F_w, \tag{1}$$

where m is the mass of pipe per unit length, t is the time, and N_x is the axial force.

$$Q = \frac{\partial M}{\partial x}, \tag{2}$$

$$M_b = -\mathrm{EI}\frac{\partial^2 w}{\partial x^2}, \tag{3}$$

where Q is shear force, M_b is bending moment, and EI is bending stiffness.

$$K = K_0 - a\Delta T \tag{4}$$

where K_0 is the initial matrix elasticity coefficient, a is its coefficient varying with temperature, and T is the thermodynamic temperature and the unit of T is Kelvin.

F_w is composed of centrifugal force, Coriolis force, and inertia force:

$$F_w = M_f\left(U^2\frac{\partial^2 w}{\partial x^2} + 2U\frac{\partial^2 w}{\partial x\,\partial t} + \frac{\partial^2 w}{\partial t^2}\right), \tag{5}$$

where M is the mass of fluid per unit length inside the pipe.

$$N_x = N_T + N_m, \tag{6}$$

where N_m is the additional axial force caused by internal liquid pressure and N_T is the axial load caused by temperature change.

$$N_m = -pA_f \tag{7}$$

where p is fluid pressure and A_f is fluid cross-sectional area.

$$N_T = -\frac{EAa}{1-2\nu}\Delta T. \tag{8}$$

Substituting equations (2), (3), (5), (7), and (8) into (1), the vibration governing equation is obtained as follows:

$$\mathrm{EI}\frac{\partial^4 w}{\partial x^4} + \left(\mathrm{MU}^2 + \mathrm{pA}_f - N_x\right)\frac{\partial^2 w}{\partial x^2} + 2\mathrm{MU}\frac{\partial^2 w}{\partial x\,\partial t} + (M+m)\frac{\partial^2 w}{\partial t^2} + \mathrm{Kw} = 0. \tag{9}$$

3. Solution of the Governing Equation

In this paper, the dynamic stiffness method is adopted to solve the control equation. Set

$$w(x,t) = W(x)e^{i\omega t}, \tag{10}$$

where $W(x)$ is the set solution of displacement in the frequency domain, ω is natural frequency, and i is imaginary unit.

Substituting equation (10) into (9) yields

$$\mathrm{EI}\frac{\partial^4 W}{\partial x^4} + \left(M_f U^2 + pA_f - N_x\right)\frac{\partial^2 W}{\partial x^2} + 2\mathrm{i}\omega\mathrm{M}_f U\frac{\partial W}{\partial x} + \left(K - \omega^2\left(M_f + m\right)\right)W = 0. \tag{11}$$

The solution form can be formulated as

$$W(x) = ce^{ikx}, \tag{12}$$

where k is wave number and c is undetermined constant.

Substituting equation (12) into (11) yields

$$\mathrm{EIk}^4 - \left(M_f U^2 + \mathrm{pA}_f - N_x\right)k^2 - 2\omega\mathrm{M}_f\mathrm{Uk} + K - \omega^2\left(M_f + m\right) = 0. \tag{13}$$

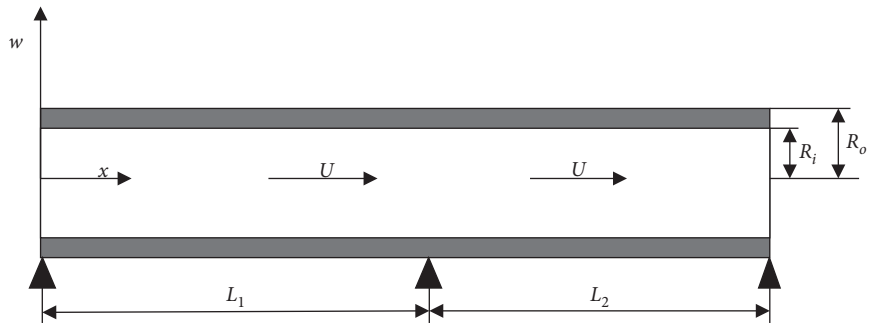

Figure 1: The model of a multispan pipe embedded in the temperature-dependent matrix.

Then, the solution of the displacement in the frequency domain can be set to

$$W(\omega, x) = \sum_{j=1}^{4} w_j e^{ik_j x}. \tag{14}$$

According to Euler–Bernoulli theory, the solutions of the rotation angle, bending moment, and shear force in frequency domain can be expressed as

$$\varphi(\omega, x) = \sum_{j=1}^{4} ik_j w_j e^{ik_j x}, \tag{15}$$

$$M(\omega, x) = \sum_{j=1}^{4} -k_j^2 \mathrm{EIw}_j e^{ik_j x}, \tag{16}$$

$$Q(\omega, x) = \sum_{j=1}^{4} \mathrm{ik}_j^3 \mathrm{EIw}_j e^{ik_j x}. \tag{17}$$

The displacement of the mth unit node of the pipeline is shown in Figure 2.

The relationship between the node displacement and the degree of freedom of the node in Figure 2 is shown as follows:

$$W_{ml} = W(0),\ \varphi_{ml} = W\prime(0),\ W_{mr} = W(l_m),\ \varphi_{mr} = W'(l_m), \tag{18}$$

$$M_{ml} = -M(0),\ Q_{ml} = -Q(0),\ M_{mr} = M(l_m),\ Q_{mr} = Q(l_m), \tag{19}$$

where l_m is the length of the mth cell node of the pipeline, subscript l represents the left end of the unit, and subscript r represents the right end of the unit.

In the local coordinate system, the node displacement of the unit can be expressed as follows:

$$\begin{Bmatrix} W_{ml} \\ \varphi_{ml} \\ W_{mr} \\ \varphi_{mr} \end{Bmatrix} = \begin{bmatrix} 1 & 1 & 1 & 1 \\ \lambda_1 & \lambda_2 & \lambda_3 & \lambda_4 \\ e^{ik_1 l_m} & e^{ik_2 l_m} & e^{ik_3 l_m} & e^{ik_4 l_m} \\ \lambda_1 e^{ik_1 l_m} & \lambda_2 e^{ik_2 l_m} & \lambda_3 e^{ik_3 l_m} & \lambda_4 e^{ik_4 l_m} \end{bmatrix} \cdot \begin{Bmatrix} w_1 \\ w_2 \\ w_3 \\ w_4 \end{Bmatrix}, \tag{20}$$

where $\lambda_j = ik_j$ $(j = 1, 2, 3, 4)$.

Equation (20) can be expressed as

$$\mathbf{W}_m = \mathbf{Y}_m(\omega)\mathbf{w}_m, \tag{21}$$

where $\mathbf{W}_m$ is the displacement vector and $\mathbf{w}_m$ is the coefficient vector.

The force of the unit node can be expressed as

$$\begin{Bmatrix} -Q_{ml} \\ -M_{ml} \\ Q_{mr} \\ M_{mr} \end{Bmatrix} = \begin{bmatrix} -\gamma_1 & -\gamma_2 & -\gamma_3 & -\gamma_4 \\ -\beta_1 & -\beta_2 & -\beta_3 & -\beta_4 \\ \gamma_1 e^{ik_1 l_m} & \gamma_2 e^{ik_2 l_m} & \gamma_3 e^{ik_3 l_m} & \gamma_4 e^{ik_4 l_m} \\ \beta_1 e^{ik_1 l_m} & \beta_2 e^{ik_2 l_m} & \beta_3 e^{ik_3 l_m} & \beta_4 e^{ik_4 l_m} \end{bmatrix} \begin{Bmatrix} w_1 \\ w_2 \\ w_3 \\ w_4 \end{Bmatrix}, \tag{22}$$

where $\gamma_j = \mathrm{ik}_j^3 \mathrm{EI}$ and $\beta_j = -k_j^2 \mathrm{EI}$ $(j = 1, 2, 3, 4)$.

Equation (22) can be expressed as

$$\mathbf{F}_m = \mathbf{X}_m(\omega)\mathbf{w}_m, \tag{23}$$

where $\mathbf{F}_m$ is the nodal force vector.

From equation (21) and equation (23), the relationship between the nodal force vector and the node displacement vector of the mth unit node of the pipeline can be obtained as follows:

$$\mathbf{F}_m = \mathbf{K}_m(\omega)\mathbf{W}_m, \tag{24}$$

in which

$$\mathbf{K}_m(\omega) = \mathbf{X}_m(\omega)\mathbf{Y}_m(\omega)^{-1}, \tag{25}$$

where $\mathbf{K}_m$ is the dynamic stiffness matrix of the mth unit node of the pipeline.

The dynamic stiffness matrix of the remaining subspan units can be established in the same way. The relationship between nodal displacements and nodal forces in the global coordinate system of multispan pipeline embedded in the temperature-dependent matrix can be constructed from the unit dynamic stiffness matrix, which can be shown as

$$\mathbf{K}_g(\omega)\mathbf{W}_g = \mathbf{F}_g, \tag{26}$$

where $\mathbf{K}_\mathrm{g}$ is the dynamic stiffness matrix in the global coordinate system, $\mathbf{W}_g$ is the displacement vector in the global coordinate system, and $\mathbf{F}_g$ is the nodal force vector in the global coordinate system.

Applying boundary conditions to $\mathbf{K}_\mathrm{g}$, we obtain

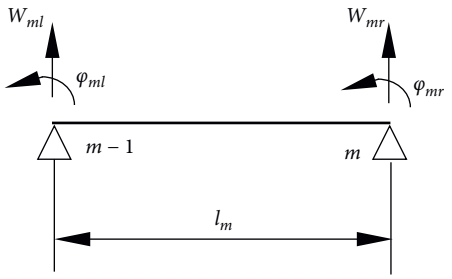

Figure 2: The displacement of the mth cell node of the pipeline.

$$\mathbf{K}_{cg}(\omega)\mathbf{W}_{cg} = \mathbf{F}_{cg}, \tag{27}$$

where the subscript cg represents the matrices and vectors that apply the boundary conditions. Set

$$h(\omega) = \det\left[\mathbf{K}_{cg}\right] = 0. \tag{28}$$

The natural frequency of the system can be obtained from the above equation. In this paper, the real part of the frequency is the vibration frequency (Re (ω)) and the imaginary part is damping (Im (ω)). The stability form of the pipeline can be divided into three situations: stable state: (Re (ω) > 0 and Im (ω) = 0), for divergence instability (Re (ω) = 0 and Im (ω) has negative value), and flutter instability (Re (ω) > 0 and Im (ω) has negative value).

4. Calculation Results and Analysis

The parameters of the pipeline, liquid, and elastic matrix are shown as follows: $L_1 + L_2 = 20m$, $R_o = 0.2\ m$, and $R_i = 0.19\ m$, the pipe density $\rho_p = 7.93 \times 10^3\ kg/m^3$, elasticity modulus $E = 2.06 \times 10^{11}\ Pa$, $v = 0.3$, the density of liquid $\rho_f = 0.8 \times 10^3\ kg/m^3$, $K_0 = 1 \times 10^5\ N/m$, and $a = 5000\ N/(m \times K)$.

In order to verify the correctness of the calculation results in this paper, the data used in the study of Deng et al. [17] are substituted into the calculation program used in this paper, and we can get the results shown in Table 1. It can be seen from the table that the results are highly consistent, which proves the correctness of the calculation in this paper.

In order to study the influence of temperature change on the first three order vibration frequency, critical velocity, and stability of the multispan pipeline embedded in the temperature-varying matrix and the influence of velocity change on the natural frequency and stability of the pipeline, we take $p = 0$, $L_1 = 10\ m$, and $L_2 = 10\ m$, and the results are shown in Figure 3 and Table 2.

By comprehensively analysis, Figure 3 obtains that, as the velocity increases, when the real part of the first-order natural frequency of the pipeline decreases to zero, the corresponding flow velocity is the critical velocity. When it reaches critical velocity, Im (ω) starts to have negative values, so this velocity is also the velocity at which the first-order divergence instability occurs. As the velocity continues to increase, the second-order natural frequency of the system decreases to 0, and the velocity is the second-order critical velocity. Further increase of the flow velocity will lead to the simultaneous occurrence of the first-order and second-order divergence instability of the system.

When $\Delta T = 0$ and $U = 0$, the first-order natural frequency is 55 Hz, the second-order natural frequency is 81 Hz, and the third-order natural frequency is 201 Hz. When $\Delta T = 0$, the first-order critical velocity is 252 m/s, the second-order critical velocity is 344 m/s, the maximum value of first-order imaginary value is 50 iHz, and the maximum value of second-order imaginary value is 43 iHz. When $\Delta T = 10$ K and $U = 0$, the first-order natural frequency is 48 Hz, the second-order natural frequency is 76 Hz, and the third-order natural frequency is 195 Hz. When $\Delta T = 10$ K, the first-order critical velocity is 220 m/s, the second-order critical velocity is 320 m/s, and the maximum value of first-order imaginary value is 52 iHz, the maximum value of second-order imaginary value is 49 iHz. When $\Delta T = 20K$ and $U = 0$, the first-order natural frequency is 39 Hz, the second-order natural frequency is 70 Hz, and the third-order natural frequency is 190 Hz. When $\Delta T = 20$ K, the first-order critical velocity is 180 m/s, the second-order critical velocity is 296 m/s, the maximum value of first-order imaginary value is 55 iHz, and the maximum value of second-order imaginary value is 55 iHz.

The above data shows that, with the increase of temperature, the value of the first three natural frequencies of the pipeline will decrease when the velocity is 0, and the critical velocity of the first-two orders will also decrease. Moreover, the first-order natural frequency decreases more obviously than the second-order and third-order natural frequency, and the first-order critical velocity decreases more obviously than the second-order critical velocity. The imaginary value of the system will change with the change of temperature, but the form of instability of the system is always static. With the increase of temperature change, the first-two imaginary values gradually approach and eventually merge together.

In order to study the influence of temperature change on the critical pressure of the multispan pipeline embedded in the temperature-varying matrix and the influence of pressure change on the natural frequency and stability of the pipeline, we take $U = 0$, $L_1 = 10m$, and $L_2 = 10m$, and the results are shown in Figure 4 and Table 2.

When $\Delta T = 0$ and $p = 0$, the first-order natural frequency is 55 Hz, the second-order natural frequency is 81 Hz, and the third-order natural frequency is 201 Hz. When $\Delta T = 0$, the first-order critical pressure is 5.1×10^7 N/m^2, the second-order critical pressure is 9.3×10^7 N/m^2, the maximum value of first-order imaginary value is 53 iHz, and the maximum value of second-order imaginary value is 22 iHz. When $\Delta T = 10$ K and $p = 0$, the first-order natural frequency is 48 Hz, the second-order natural frequency is 76 Hz, and the third-order natural frequency is 195 Hz. When $\Delta T = 10$ K, the first-order critical pressure is 3.85×10^7 N/m^2, the second-order critical pressure is 8.15×10^7 N/m^2, the maximum value of first-order imaginary value is 61 iHz, and the maximum value of second-order imaginary value is 37 iHz. When $\Delta T = 20$ K and $p = 0$, the first-order natural frequency is 39 Hz, the second-order natural frequency is 70 Hz, and the third-order natural frequency is 190 Hz. When $\Delta T = 20$ K, the first-order critical

Table 1: Dimensionless natural frequency comparison ($p = 0$).

Dimensionless flow velocity	Dimensionless natural frequency	In this paper	Deng et al. (2017)
$U = 0$	ϖ_1	21.33	21.33
	ϖ_2	70.42	70.41
	ϖ_3	147.96	147.91
$U = 1.5$	ϖ_1	20.24	20.24
	ϖ_2	69.52	69.52
	ϖ_3	147.08	147.04

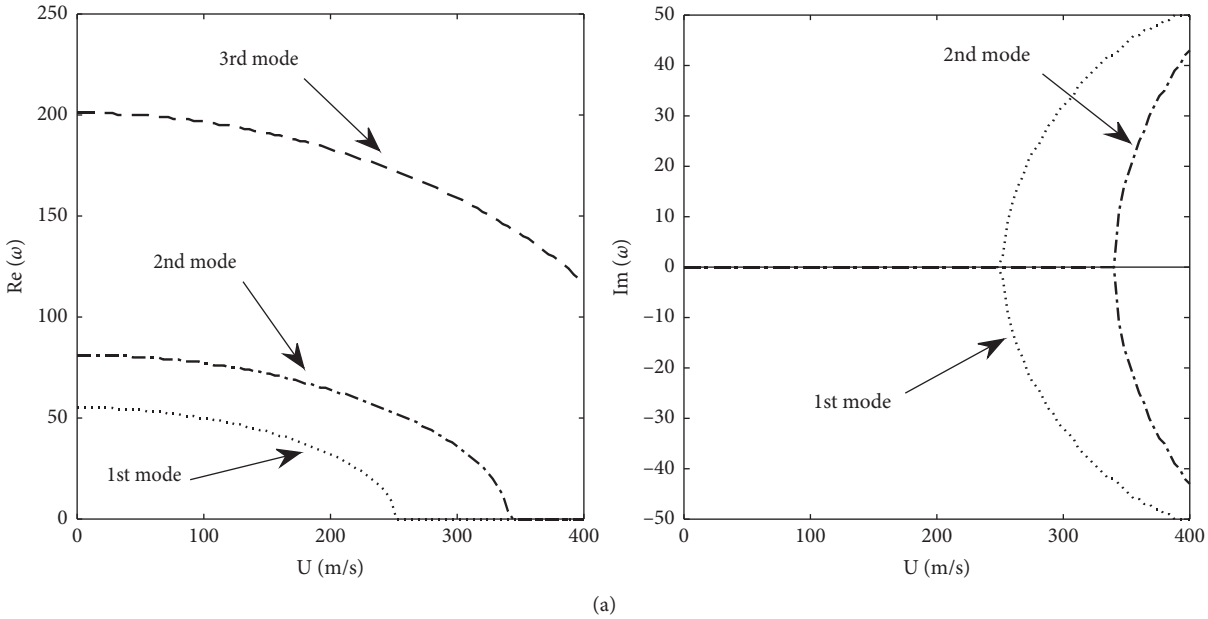

(a)

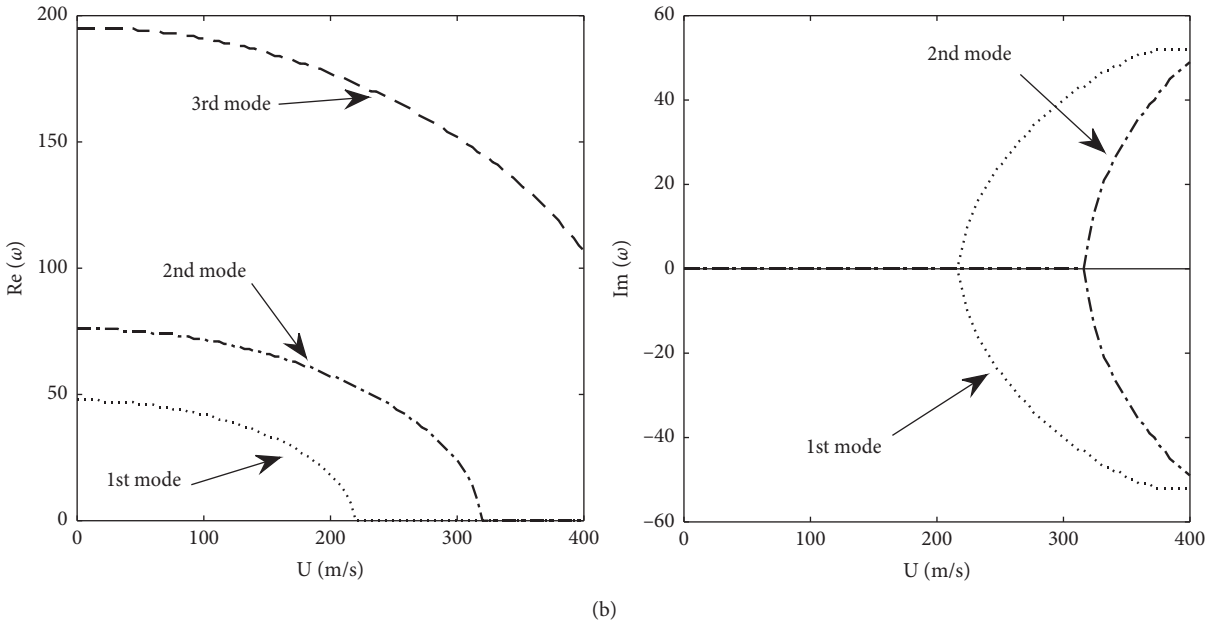

(b)

Figure 3: Continued.

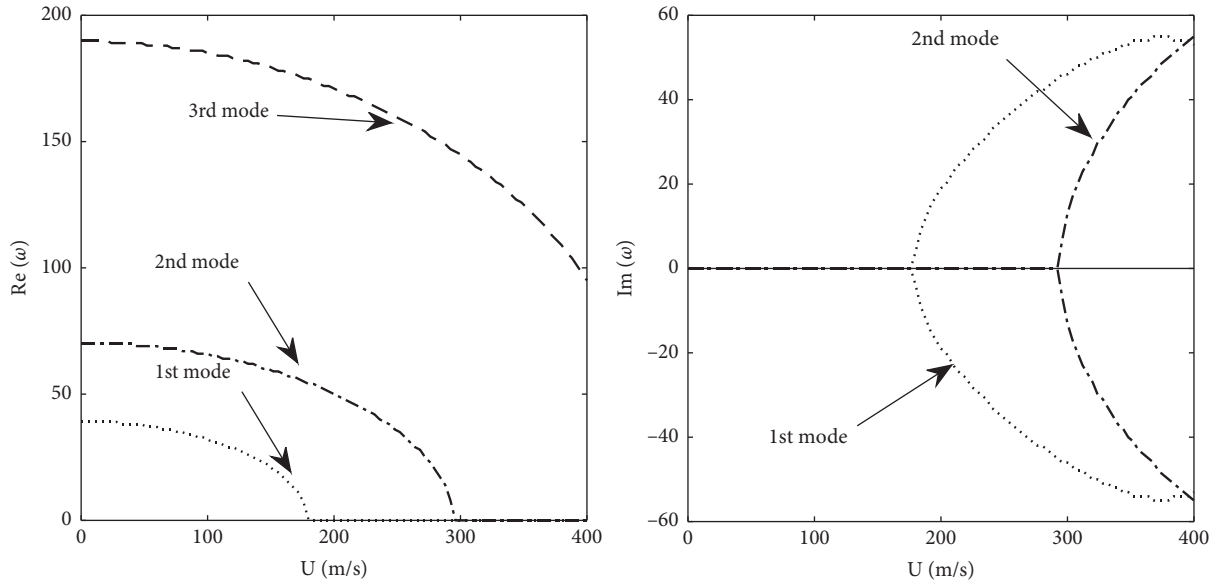

(c)

Figure 3: Frequency varies with flow velocity: (a) $\Delta T = 0$, (b) $\Delta T = 10$ K, and (c) $\Delta T = 20$ K.

Table 2: The key point data of Figures 3 and 4.

Temperature variation	Natural frequency $U = 0$, $p = 0$ (Hz)	Critical velocity (m/s)	Critical pressure (N/m^2)
$\Delta T = 0$	1st order 55 2nd order 81 3rd order 201	1st order 252 2nd order 344	1st order 5.1×10^7 2nd order 9.3×10^7
$\Delta T = 10$ K	1st order 48 2nd order 76 3rd order 195	1st order 220 2nd order 320	1st order 3.85×10^7 2nd order 8.15×10^7
$\Delta T = 20$ K	1st order 30 2nd order 70 3rd order 190	1st order 180 2nd order 296	1st order 2.6×10^7 2nd order 6.95×10^7

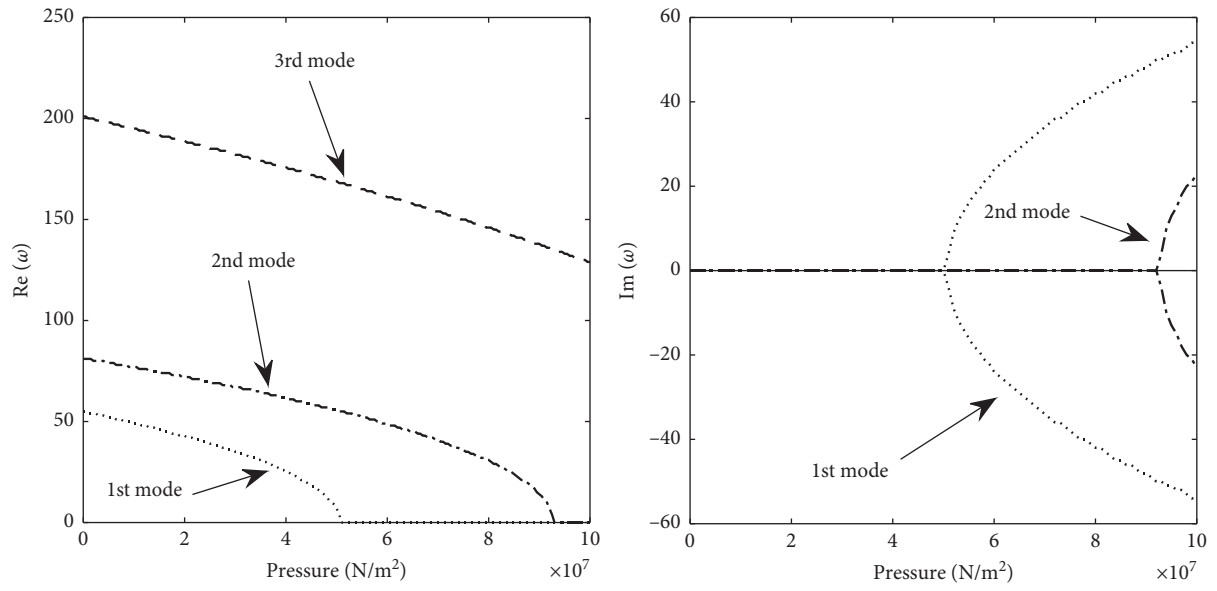

(a)

Figure 4: Continued.

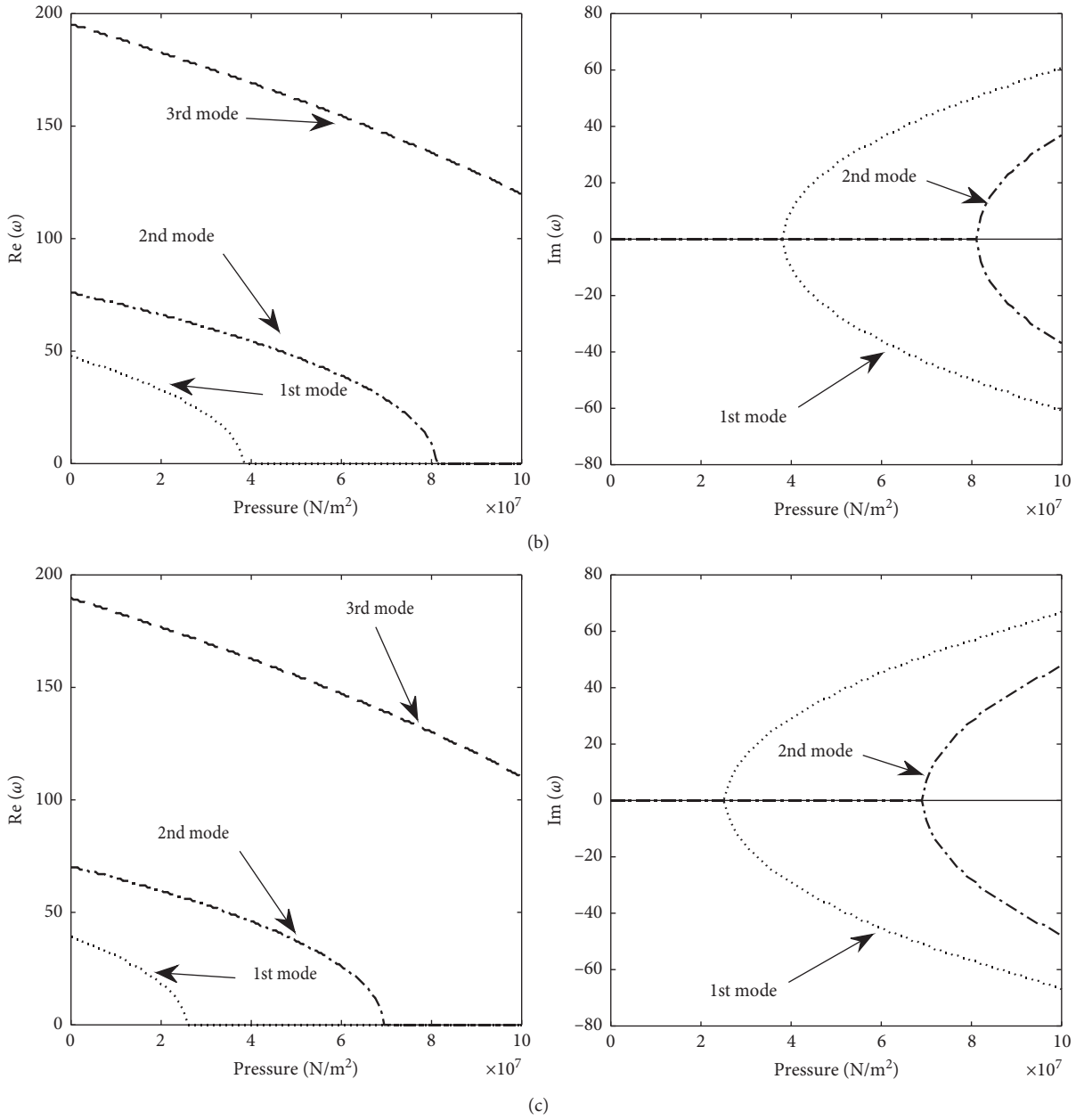

Figure 4: Frequency varies with pressure: (a) $\Delta T = 0$, (b) $\Delta T = 10$ K, and (c) $\Delta T = 20$ K.

pressure is 2.6×10^7 N/m^2, the second-order critical pressure is 6.95×10^7 N/m^2, the maximum value of first-order imaginary value is 67 iHz, and the maximum value of second-order imaginary value is 48 iHz.

By comprehensively analysis, Figure 4 obtains that the influence of internal pressure change on system stability is basically the same as that of flow velocity. With the increase of pressure in the pipe, when Re (ω) decreases to zero, the corresponding pressure is critical pressure. The critical pressure is also the pressure of its first-order divergence instability. As the pressure continues to increase, the second-order natural frequency of the system decreases to 0, and the pressure at this time is the second-order critical pressure. If the pressure continues to increase, the first- and second-order divergence instability of the system will occur simultaneously.

The effect of temperature change on critical pressure is similar to that on critical velocity. And, the first and second critical pressure decrease obviously with the increase of temperature. The imaginary value of the system will change with the change of temperature, but the form of instability of the system is always divergence instability. With the increase of temperature, the imaginary values of the first two orders have no tendency to get closer.

In order to make the results of Figures 3 and 4 more intuitive, the data results of Figures 3 and 4 are summarized as Table 2.

In order to study the influence of different span combinations on critical pressure, critical velocity, natural frequency, and stability of the multispan pipeline embedded in the temperature-varying matrix, we take $T = 0$, and the results are shown in Figure 5 and Table 3.

When $L_1 = 10$ m, $L_2 = 10$ m, $U = 0$, and $p = 0$, the first-order natural frequency is 55 Hz, the second-order natural frequency is 81 Hz, and the third-order natural frequency is 201 Hz. When $L_1 = 10$ m and $L_2 = 10$ m, the first-order critical velocity is 252 m/s, the second-order critical velocity is 344 m/s, the first-order critical pressure is 5.1×10^7 N/m^2, and the second-order critical pressure is 9.3×10^7 N/m^2. When $L_1 = 10m$, $L_2 = 10m$, and $U = 400$ m/s, the maximum imaginary of the first-two orders occurs, the maximum value of first-order imaginary value is 50 iHz, and the maximum value of second-order imaginary value is 43 iHz. When $L_1 = 10$ m, $L_2 = 10$ m, and $p = 10 \times 10^7$ N/m^2, the maximum imaginary of the first-two orders occurs, the maximum value of first-order imaginary value is 53 iHz, and the maximum value of second-order imaginary value is 22 iHz. With the increase of velocity and pressure, the value of imaginary changes in the parabolic form.

When $L_1 = 12$ m, $L_2 = 8$ m, $U = 0$, and $p = 0$, the first-order natural frequency is 48 Hz, the second-order natural frequency is 100 Hz, and the third-order natural frequency is 163 Hz. When $L_1 = 12$ m and $L_2 = 8$ m, the first-order critical velocity is 252 m/s, the second-order critical velocity is 348 m/s, the first-order critical pressure is 5.05×10^7 N/m^2, and the second-order critical pressure is 9.65×10^7 N/m^2. When $L_1 = 12$ m, $L_2 = 8$ m, and $U = 400$ m/s, the maximum value of the imaginary is 47 iHz; when $U = 356$ m/s, there is an obvious inflection point in the first-order imaginary change diagram, where the second-order imaginary occurs and coincides with the first-order imaginary. When $L_1 = 12$ m, $L_2 = 8$ m, and $p = 10 \times 10^7$ N/m^2, the maximum imaginary of the first-two orders occurs, the maximum value of first-order imaginary value is 49 iHz, the maximum value of the second-order imaginary value is 20 iHz; with the increase of pressure, the value of imaginary changes in the parabolic form.

When $L_1 = 16$ m, $L_2 = 4$ m, $U = 0$, and $p = 0$, the first-order natural frequency is 35 Hz, the second-order natural frequency is 92 Hz, and the third-order natural frequency is 188 Hz. When $L_1 = 16$ m and $L_2 = 4$ m, the first-order critical velocity is 248 m/s, the second-order critical velocity is 332 m/s, the first-order critical pressure is 4.9×10^7 N/m^2, and the second-order critical pressure is 9.05×10^7 N/m^2. When $L_1 = 16$ m, $L_2 = 4$ m, and $U = 400$ m/s, the maximum value of imaginary value is 46 iHz; when $U = 332$ m/s, there is an obvious inflection point in the first-order imaginary change diagram, where the second-order imaginary occurs and coincides with the first-order imaginary. When $L_1 = 16$ m, $L_2 = 4$ m, and $p = 10 \times 10^7$ N/m^2, the maximum imaginary of the first-two orders occurs, the maximum value of the first-order imaginary value is 44 iHz, and the maximum value of the second-order imaginary value is 25 iHz; with the increase of pressure, the value of imaginary changes in the parabolic form.

By comprehensively analysis Figure 5 obtains that different span combinations have little influence on the first-order critical velocity. When the span combination is 16 m + 4 m, the second-order frequency of the system does not decrease to zero, which is obviously different from the previous two span combinations. The increase of the length of the first section of the pipeline will lead to the decrease of the first-order critical pressure of the system, but the change rule of the second-order critical pressure is not obvious. In addition, among the three span combinations, the 12 m + 8 m span combinations have the highest second-order critical pressure, and the 16 m + 4 m span combinations have the lowest second-order critical pressure. When $U = 0$ and $T = 0$, with the first section of the pipeline length increasing and the length of the second section of the pipeline decreasing, the first-order natural frequency will decrease, but the system of second-order natural frequency will increase after the first decreases, and the change law of the third-order natural frequency is opposite with the second-order natural frequency. As the flow velocity increases, different span combinations will eventually lead to the instability form of the system change. When the span combinations is 10 m + 10 m, the first-order divergence instability of the system will occur, and then the first and second-order divergence instability will occur. When the span combinations are 12 m + 8 m, the divergence instability of the system will occur. With the increase of flow velocity, the first-order imaginary change rule of the absolute value is that it first increases then decreases and then increases and the second-order imaginary will appear and will soon coupled with the first-order imaginary. It will eventually lead to the divergence instability of the system under the coupling of the first and second modes. When the span combinations is 16 m + 4 m, the instability form of the system will be different from the previous two. The second-order natural frequency of the system does not change to 0, which can lead to flutter instability of the system. With the increase of flow velocity, the first-order imaginary change rule of the absolute value is that it first increases then decreases and then increases and the second-order imaginary will appear and will soon coupled with the first-order imaginary. Finally, the system will change from divergence instability to flutter instability under the coupling of the first and second modes.

With the increase of pipeline internal pressure, the instability forms caused by different span combinations are exactly the same, which are the first divergence instability in the first-order mode, and then there is the divergence instability in the first-order mode and the second-order mode at the increase of internal pressure.

In order to make it easier for readers to understand the instability modes changes of pipelines with different span combinations, we summarize the instability modes and critical points in Figure 5 and Table 3.

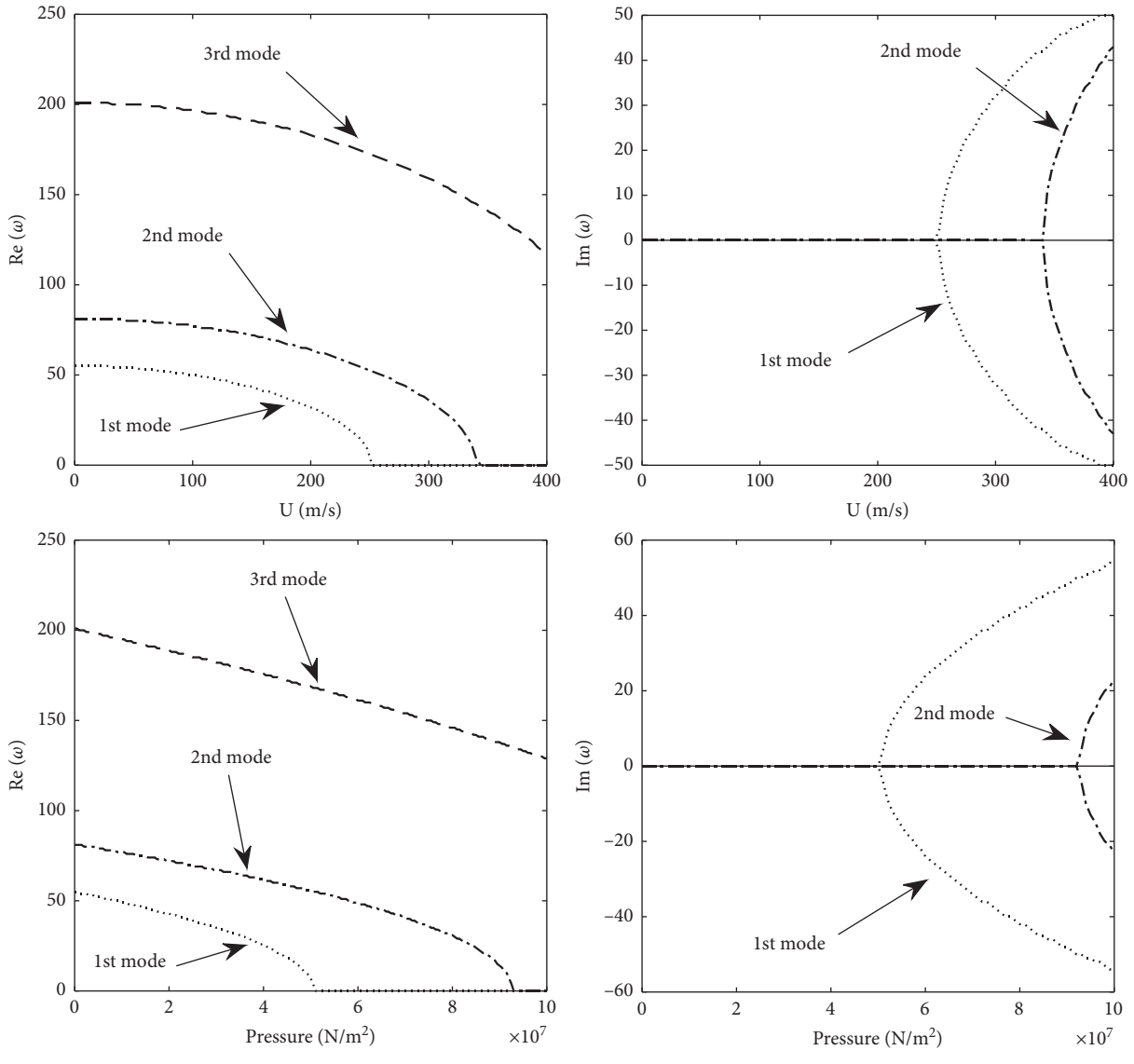

(a)

Figure 5: Continued.

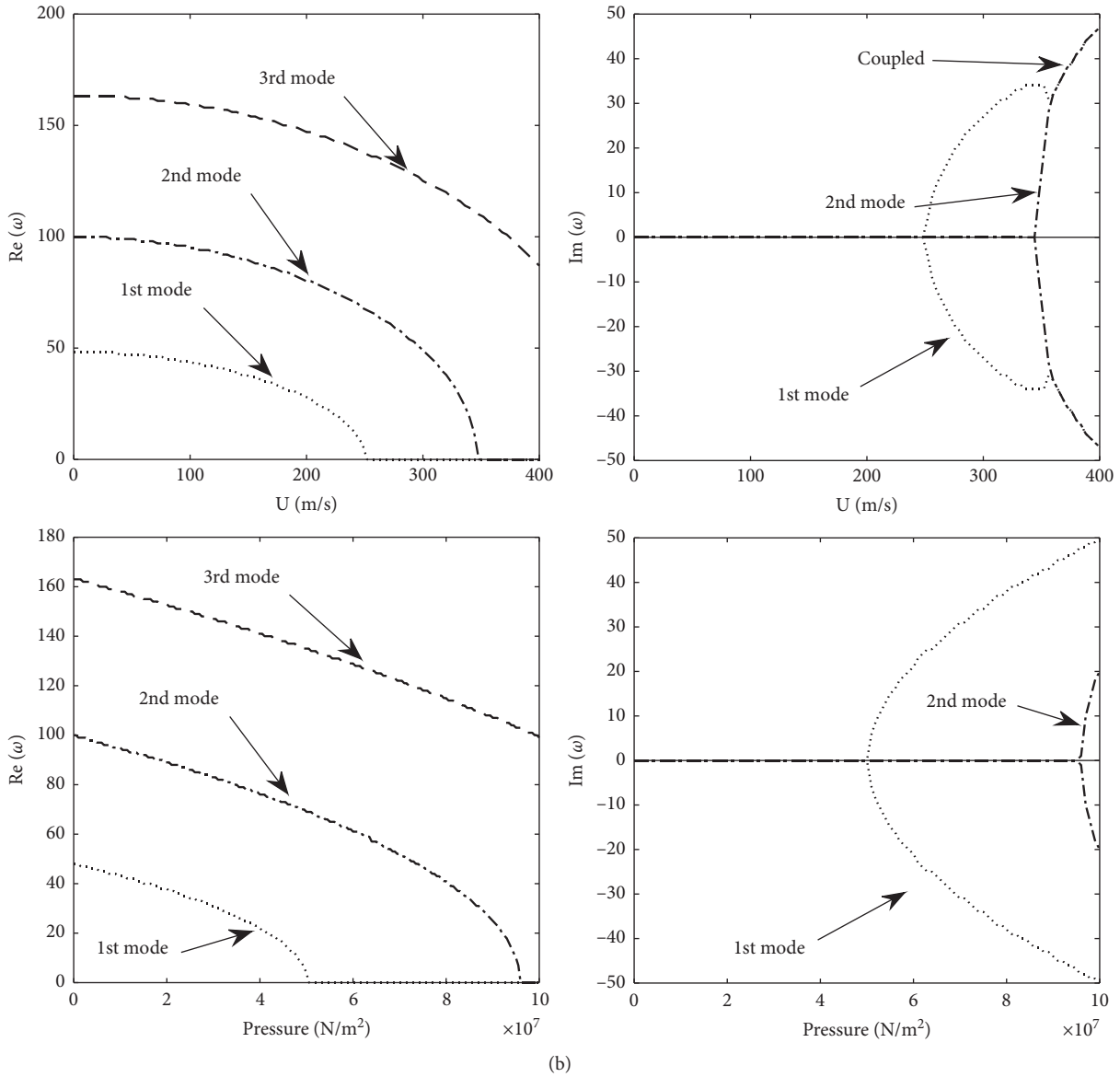

(b)

Figure 5: Continued.

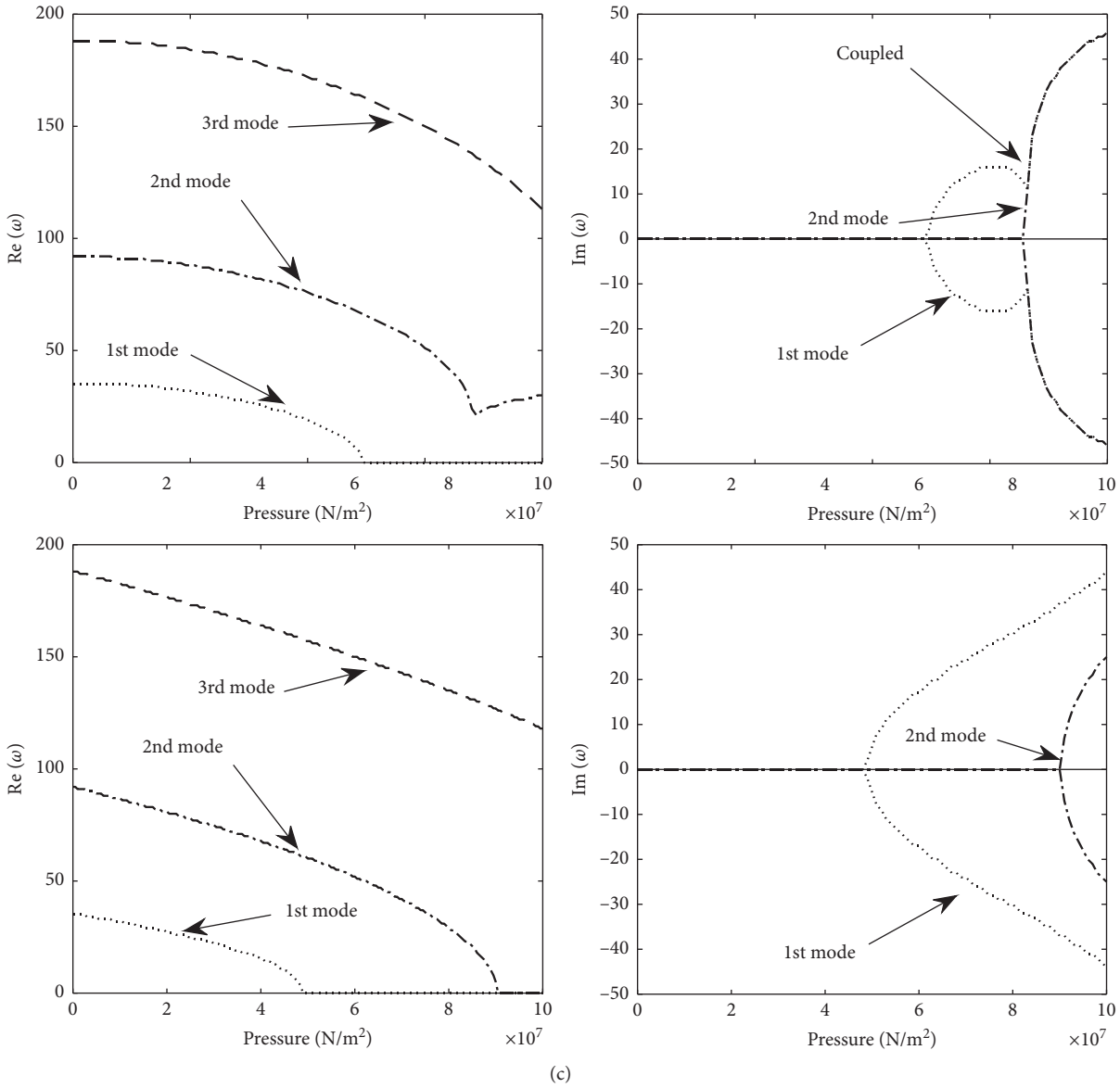

Figure 5: Different span combinations: (a) 10 m + 10 m, (b) 12 m + 8 m, and (c) 16 m + 4 m.

Table 3: Instability modes and critical points under different span combinations.

Span combination	Instability mode (U m/s)	Instability mode (p N/m^2)
$L_1 = 10\,m$, $L_2 = 10\,m$	1st order divergence instability 252	1st order divergence instability 5.1×10^7
	1st and 2nd order divergence instability 344	1st and 2nd order divergence instability 9.3×10^7
$L_1 = 12\,m$, $L_2 = 8\,m$	1st order divergence instability 252	1st order divergence instability 5.05×10^7
	1st and 2nd order coupling divergence instability 348	1st and 2nd order divergence instability 9.65×10^7
$L_1 = 16\,m$, $L_2 = 4\,m$	1st order divergence instability 248	1st order divergence instability 4.9×10^7
	1st and 2nd order coupling flutter instability 332	1st and 2nd order divergence instability 9.05×10^7

5. Conclusions

Through summarizing and sorting out the results of this paper, the conclusions are shown as follows:

(1) The increase of temperature will lead to the reduction of the first three natural frequencies of the system when the flow velocity and pressure are 0, among which the first natural frequency decreases most obviously. The increase of the temperature also leads to a significant decrease in the first-two order critical flow velocity and pressures, and the decrease in the first critical flow velocity is more obvious than that in the second. The increase of the temperature has a certain influence on the change of imaginary value, but it does not change the mode of system instability.

(2) The change of span combinations has little influence on the first-order critical velocity and first-order critical pressure of the system. However, it will cause the second-order critical pressure and the velocity of the system change. When $U = 0$ and $T = 0$, the first-order natural frequency of the system obviously increases and then decreases as the length of the first pipe increases, but the second-order and third-order natural frequency changes have no such phenomena.

(3) The increase of flow velocity will lead to the change of the instability form of different span combination systems, while the pressure change in the pipeline will not lead to the change of the instability form of different span combinations.

Data Availability

The data used to support the findings of the study are available from the corresponding author upon request.

Conflicts of Interest

The authors declare that they have no conflicts of interest.

References

[1] M. P. Païdoussis and G. X. Li, "Pipes conveying fluid: a model dynamical problem," *Journal of Fluids and Structures*, vol. 7, pp. 137–204, 1993.

[2] R. A. Ibrahim, "Overview of mechanics of pipes conveying fluids-Part I: fundamental studies," *Journal of Pressure Vessel Technology*, vol. 132, pp. 1–32, 2010.

[3] S. Li, B. W. Karney, and G. Liu, "FSI research in pipeline systems - a review of the literature," *Journal of Fluids and Structures*, vol. 57, pp. 277–297, 2015.

[4] Z. Zhang, Y. Liu, and T. Han, "Two parameters affecting the dynamics characteristics of a uniform conical assembled pipe conveying fluid," *Journal of Vibration and Control*, vol. 23, pp. 361–372, 2017.

[5] Q. Ni, Y. Luo, M. Li, and H. Yan, "Natural frequency and stability analysis of a pipe conveying fluid with axially moving supports immersed in fluid," *Journal of Sound and Vibration*, vol. 403, pp. 173–189, 2017.

[6] B. H. Li, H. S. Gao, Y. S. Liu, and Z. F. Yue, "Transient response analysis of multi span pipe conveying fluid," *Journal of Vibration and Control*, vol. 19, pp. 2164–2176, 2013.

[7] T.-Z. Yang, X.-D. Yang, Y. Li, and B. Fang, "Passive and adaptive vibration suppression of pipes conveying fluid with variable velocity," *Journal of Vibration and Control*, vol. 20, no. 9, pp. 1293–1300, 2013.

[8] Y. Xu and Z. Jiao, "Exact solution of axial liquid-pipe vibration with time-line interpolation," *Journal of Fluids and Structures*, vol. 70, pp. 500–518, 2017.

[9] G. H. Chang and Y. Modarres-Sadeghi, "Flow-induced oscillations of a cantilevered pipe conveying fluid with base excitation," *Journal of Sound and Vibration*, vol. 333, no. 18, pp. 4265–4280, 2014.

[10] M. F. Lumentut and M. I. Friswell, "A smart pipe energy harvester excited by fluid flow and base excitation," *Acta Mechanica*, vol. 229, no. 11, pp. 4431–4458, 2018.

[11] T. Elaikh, S. Hmod, and E. Bustan, "Dynamic behavior of cracked functionally graded (FG) material pipe conveying fluid," *International Journal of Energy and Environment*, vol. 9, no. 6, pp. 591–606, 2018.

[12] Z.-M. Wang and Y.-Z. Liu, "Transverse vibration of pipe conveying fluid made of functionally graded materials using a symplectic method," *Nuclear Engineering and Design*, vol. 298, pp. 149–159, 2016.

[13] J. Cao, Y. Liu, and W. Liu, "The effect of two cases of temperature distributions on vibration of fluid-conveying functionally graded thin-walled pipes," *The Journal of Strain Analysis for Engineering Design*, vol. 53, no. 5, pp. 324–331, 2018.

[14] M. Raminnea, H. Biglari, F. V. Tahami, and M. Raminnea, "Nonlinear higher order Reddy theory for temperature-dependent vibration and instability of embedded functionally graded pipes conveying fluid-nanoparticle mixture," *Structural Engineering and Mechanics*, vol. 59, no. 1, pp. 153–186, 2016.

[15] L. Wang and Q. Ni, "A reappraisal of the computational modelling of carbon nanotubes conveying viscous fluid," *Mechanics Research Communications*, vol. 36, no. 7, pp. 833–837, 2009.

[16] M. Sadeghi-Goughari, S. Jeon, and H.-J. Kwon, "Flutter instability of cantilevered carbon nanotubes caused by magnetic fluid flow subjected to a longitudinal magnetic field," *Physica E: Low-Dimensional Systems and Nanostructures*, vol. 98, pp. 184–190, 2018.

[17] J. Deng, Y. Liu, Z. Zhang, and W. Liu, "Stability analysis of multi-span viscoelastic functionally graded material pipes conveying fluid using a hybrid method," *European Journal of Mechanics - A/Solids*, vol. 65, pp. 257–270, 2017.